Mathematical formulation for the analysis of the periodic convergence during co-processing routines in long-run, scale-resolving simulations of turbomachinery

Jesús Manuel Fernández-Oro*

Fluid Mechanics Area of the Energy Department,
Gijón Polytechnic School of Engineering, University of Oviedo.
Department Building East Zone, Campus of Viesques, 33203, Gijón, Spain.
Email: jesusfo@uniovi.es
*Corresponding author.

Abstract: Scaled-Resolving Simulations, like LES modelling, are recent CFD techniques to analyse numerically unsteady flows and turbulence in turbomachinery. Despite their high computational costs, they provide an unsteady, time-resolved solution of the flow with embedded turbulent scales. From an engineering point-of-view, a statistical description of such solutions is mandatory. Thus, phase-averaged values of velocity fields and turbulent scales must be postprocessed in order to provide a representative description of the unsteadiness, using a minimum number of averages that it is a priori unknown. This required number depends on the flow complexity, the type of turbomachine and its operating condition.
In order to save computational costs, the present paper provides the mathematical formulation required to compute and assure that periodic convergence has been met. The framework has been developed to update the phase-averaged values and the residual on the run, so the amount of data to be stored is extremely reduced. Following, the formulation is applied over a previous numerical database concerning a Wall-Modelled LES simulation of the Rotor-Stator Interaction in a low-speed axial fan using a 3D linear cascade model. The results obtained confirm that convergence of turbulent structures is more compromised than primary flow variables due to inherent instabilities of the coherent flow vortices.
This work forms part of the concept of co-processing, in which some operations related to post-processing routines are moved towards the iterative resolutions processes of numerical CFD simulations in order to save computational costs.

Keywords: Statistical convergence, co-processing, phase-averaging, LES simulation, Rotor-Stator interaction, axial fan

Reference to this paper should be made as follows: Fernández-Oro, J.M. (2020) 'Mathematical formulation for the analysis of the periodic convergence during co-processing routines in long-run, scale-resolving simulations of turbomachinery', *Progress in Computational Fluid Dynamics*, Vol. X, No. Y4, pp.000–000.

Biographical notes: Jesús Manuel Fernández Oro is an Associate Professor (since 2010) in the Fluid Mechanics Area of the Energy Department at the University of Oviedo. He received his MSc Degree in Mechanical Engineering at the Polytechnic Engineering School of Gijón (2000) and his PhD at the University of Oviedo with the thesis dissertation entitled "Unsteady Rotor-Stator Interaction in a Low-Speed Axial Flow Fan" (2005). His current research activities are mainly focused on (1) the analysis and description of turbulence and unsteady flows in turbomachinery, (2) the development and application of measurement and visualization techniques in experimental Fluid Mechanics and (3) CFD modelling and numerical simulation of fluid machinery.

1 Introduction

Unsteady Reynolds-Averaged Navier-Stokes (URANS) modelling is the standard approach for the CFD simulation of incompressible flows in turbomachinery applications. With this level of fidelity, in which all turbulent phenomena are modelled, global parameters like the pressure rise or the mean-time efficiency can be reasonably obtained, especially at nominal or close-to-nominal conditions. However, the existence of a spectral gap between the turbulent time scales (integral time scale) and the large-scale fluctuations associated with the blade passing frequency (BPF) is required; a critical aspect which is not usually guaranteed (Tucker, 2011).

To overcome this problem, Scale-Resolving Simulations (SRS), (Menter, 2015), also known as Eddy-Resolving

Simulations, ERS (Tucker and Tyacke, 2016) have progressively emerged as an enhanced option to simulate unsteady flows and turbulence in multistage turbomachinery with higher accuracy. These methods resolve all or just a part of the turbulence spectrum in at least a portion of the numerical domain. Large Eddy Simulation (LES) is the most popular technique but other formulations including hybrid RANS/LES schemes have been recently developed to simulate both global and local unstable flows (Lehnhauser et al., 2004); (Benim et al., 2011). The Scale Adaptive Simulation (SAS), that precludes the formation of broadband turbulence, the Detached Eddy Simulation (DES) or Wall-Modelling LES (WMLES), especially developed for wall-bounded flows and the Embedded LES (ELES) for zonal, massive separations are examples of such hybrid schemes.

All these scale-resolving methodologies, using the LES technique as cornerstone, provide a highly accurate description of time-dependent physics of the turbulent motion. Unfortunately, the computational costs and CPU times required are still a limiting factor that prevents classic RANS modelling from being abandoned.

In turbomachinery environments, non-linear and viscous phenomena related to wake-blade and wake-wake interactions arise within the passages, resulting in extremely complex flow patterns with multiple length scales. RANS turbulence models can predict turbulence generation, wake flow and even mild separation but fails in the description of turbulent mixing in high-swirl vortical structures (Javadi and Nilsson, 2015). This is especially critical in the case of turbomachinery flows with heat transfer, involving non-uniform density distributions and time-dependent hot-spots (Adamczyk, 1999); (Chow et al., 2002). Under such conditions, the assumption of a spectral gap between turbulent structures and large-scale fluctuations is no longer valid, so the use of URANS modelling, supported by this separation of scales, should be avoided.

In the case of incompressible flow turbomachinery (typically, centrifugal pumps and low-pressure fans or blowers) these constraints are relaxed with less intense interactions and reduced turbulent mechanisms, specially at design conditions. Deterministic oscillations (Meneveau and Katz, 2002) are predominant, so URANS modelling can still provide reliable estimations (Huang et al., 2010); (Ziegler, 2017). However, at off-design conditions (especially near stall/surge margins), scale-resolving techniques are desirable and should be employed to simulate accurately the convective transport of vortical structures (eddies), despite the computational costs (Tucker, 2011b and Gourdain et al., 2014). A correct description of these eddies is essential to simulate accurately the response of blades and vanes boundary layers in multistage environments, which allows a precise prediction of their time-averaged performance.

Extremely fine meshes and low time steps are severe constraints in LES-based simulations, with temporal and spatial discretizations that should be 10^3 to 10^4 times denser than URANS simulations (Michelassi, 2013). Fortunately, for the simulation of blade-to-blade passages at midspan locations in turbomachinery (i.e., decoupling endwall casings), the computational requirements can be notably relaxed using hybrid methods (WMLES for shear layer flows in the blade surfaces and/or ELES for highly-detached flow regions). It is known that coherent turbulent structures are mainly confined to streamwise planes, so 3D spanwise-restricted models with only a portion of the blade span (5-10% of the blade chord) are a reasonable approach for the economic analysis of these flows. These simulations, typically with a few millions cells (in the order of 1 million elements per passage for Reynolds numbers in the range of $10^5 – 10^6$) (Tucker, 2011c) are currently affordable and allow the use of scale-resolving methods even for industrial manufacturers and designers.

In addition, the solution of LES-based simulations provides an inherent, time-dependent description of the flow fields which complicates the classic idea of numerical convergence. Superimposed on the (partially) resolved turbulence, the periodic variation of the flow due to the unsteady blade rotation involves the necessity for statistical post-processing of the results. Hence, not only a spatial-filtering average must be introduced in the pre-processing of the numerical solution (to provide the LES set of equations to be resolved), but also a phase-averaging is required in the post-processing for an accurate and practical statistical description of the turbulent motions. Obviously, this leads to the generation of large amounts of data to be post-processed, which is an additional problem of CPU time and high computational costs for CFD users.

To handle this data, co-processing (Duan, 2014), is emerging as the most cost-effective way to process relevant data, where runtime in-memory processing of the flow is occurring concurrently to the simulation itself. In the case of LES-based simulation of turbomachinery flows, it is necessary to decide in an aprioristic basis which is the region of interest, update statistics on the fly and store only this co-processed statistical data. Convergence is judged upon this data and finally written for definitive post-processing.

In this paper, the mathematical expressions required to perform these co-processed statistics on the run are derived and discussed in detail. A mathematical framework, based on the phase-averaging operator clocked with the blade passing frequency, is firstly exploited to provide first-order and second-order statistics that assures the deterministic convergence of turbomachinery flows. Additionally, a numerical database from a low-speed axial fan (Fernández Oro et al, 2019) using a LES-based model is presented and employed to use these expressions during the convergence procedure. This mathematical framework allows a notable reduction of the number of transient computations for SRS modelling and helps advanced users of CFD codes to save CPU time and guarantee reliable periodic convergence.

2 Time scales and spectral gap

From an engineering point of view, the description of the time-resolved turbulent flow is essential for an accurate simulation of the energy transfer within the passages of any turbomachine. The vortical dynamics of the wake fluid, being

convected by the streamwise velocity, in combination with the large gradients arising due to the blade motion and with complex rotor-stator interactions between adjacent blade/vane rows, provokes a wide range of temporal scales in the unsteady flow patterns.

Typically, the instantaneous value of any variable can be decomposed into a time-averaged value, a deterministic fluctuation related to the blade passing period (t_{BPF}) and turbulent instabilities with highest time scales (t_{ILS}) in the order of those of the integral eddies. These random fluctuations range from the integral eddy size (or length scales, ILS) down to the Kolmogorov dissipation scales (t_{KOL}). The existence of a spectral gap requires that $t_{BPF} \gg t_{ILS}$, or equivalent to $f_{ILS}/f_{BPF} \gg 1$. However, this condition is not commonly satisfied, especially for the turbomachines with significant rotating speeds (above 1500-2000 rpm) and a large number of blades per rotor row (above 5-7).

In a rotor-stator configuration, additional important time scales introduce more complexity into the flow description. Vortex shedding mechanisms of the wake flow coming from upstream rows (t_{SHED}) as well as the vortical dynamics evolving in the boundary layer of the row of interest (t_{BL}) are also convected, contributing to enhance the turbulent mixing. Tucker (2011b, 2011c) provides an in-depth review of these time scales for engine gas turbines.

Figure 1 shows a sketch of all these turbulent scales from the representation of the unsteady vorticity maps at a given instant in the interrow region of a one stage, low-speed axial fan. These maps have been taken from the results of a LES-based simulation of an axial fan (Fernández Oro et al, 2019) designed to resolve roughly 70% of the turbulent energy budget in the vicinity of the rotor blades (More details of the simulation are presented later in section 4). Both nominal (top) and off-design (bottom) conditions are shown in Figure 1. The different turbulent motions and interaction mechanisms are illustrated and conceptually identified in the figure. The periodic impingement of upstream wakes (related to the time required for a fluid particle to pass through the blade passage, f_{FLOW}/f_{BPF}) is evident at nominal conditions, being mixed with the turbulent structures shed from the vane trailing edge (f_{BL}/f_{BPF}). At off-design conditions, the vortex shedding from the upstream blades (f_{SHED}/f_{BPF}) and the interaction triggering large-scale vortices in the suction surface of the vanes (f_{ILS}/f_{BPF}) reveals the higher complexity of the turbulence picture at partial conditions.

Figure 1 Identification of turbulent structures at nominal (top) and off-design (bottom) conditions.

Furthermore, table 1 shows a rough estimation of the relevant time scales in terms of frequency ratios with respect to the blade passing frequency (as labelled in the figure). For this database, the BPF is equal to 360 Hz (9 rotor blades and a rotational speed of 2400 rpm). Note that all mechanisms present a similar frequency range, except for the Kolmogorov scales that it is roughly two orders of magnitude higher than the rest. It is also noticeable that the eddy scales from the boundary layer of the vane at nominal conditions is significantly higher than the unsteadiness of the incoming wakes (f_{SHED}/f_{BPF}=4.83). Additionally, the condition for the spectral gap is marginally fulfilled (f_{ILS}/f_{BPF}>1) in that case, thus suggesting that a URANS simulation of the nominal condition can be considered. Conversely, at off-design conditions, the generation of large-scale turbulence occurs more rapidly than the periodic fluctuation of the non-uniform incoming flow, thus invalidating the assumption of a spectral gap.

Table 1 Time scales of relevant turbulent and unsteady mechanisms.

R-S config.	Nominal (Q_N)	Off-design (70%Q_N)
f_{FLOW}/f_{BPF}	0.73	0.51
f_{ILS}/f_{BPF}	1.21	0.67
f_{SHED}/f_{BPF}	4.83	1.51
f_{BL}/f_{BPF}	2.41	1.69
f_{KOL}/f_{BPF}	25.8	62.7

More insight regarding the spectral gap is provided in table 2, showing typical values of turbulence intensity, length scales and the corresponding frequency of the integral time scale. Previous investigations (both numerical and experimentally) have determined typical integral scales in the order of 1/15 of the blade chord for the nominal conditions and around 1/3 of the chord for near-stall conditions (Fernández Oro et al., 2019; and Galdo-Vega et al., 2013). From the turbulent kinetic energy, a characteristic velocity fluctuation U for the turbulent motion is derived and thus the large eddy "turnover" time (t_{ILS}) is estimated. This integral time scale is the specific value compared to the blade passing period in the previous table.

This is perfectly illustrated with the representation of the velocity trace and its corresponding frequency spectrum in a point close to the leading edge of the vane. Numerical results for both flow rate conditions are compared in figure 2. As expected, the temporal evolution of the velocity trace at nominal conditions (black line) reveals the scale disparity between the deterministic oscillations clocked with the BPF and the small turbulent mechanisms (the flow is very repeatable), whereas at off-design conditions, the turbulent instabilities makes it impossible to separate the scales (red line). The spectrum shows clearly how the BPF scales are completely immersed in the inertial subrange of the turbulent energy cascade when the axial fan is working at partial load (red spectrum), which makes the assumption of a spectral gap clearly controversial.

Table 2 Estimation of the integral time scale as a function of the flow rate.

R-S config.	Nominal (Q_N)	Off-design (70%Q_N)
Tu (%)	~ 10%	~ 40%
ILS	~ c/15	~ c/3

U (m/s)	~ 4	~ 12
t_{ILS} (s)	$2.3 \cdot 10^{-3}$	$4.1 \cdot 10^{-3}$
f_{ILS} (Hz)	434	244

Figure 2 Velocity traces for 10 blade events (left) in a point P close to the vane LE: nominal (top) and off-design (bottom) conditions. Comparison of fluctuating spectra (right). See the point location in the small figure.

3 Mathematical framework for periodic convergence in a LES context

Although URANS modelling is a problematic option when turbulence and deterministic unsteadiness are similar in magnitude and frequency range, an explicit decomposition between stochastic and periodic components (like URANS precludes) is still a useful scheme for the analysis of turbomachinery flows. From an engineering point of view, the introduction of statistical averaging allows one to identify the origin and nature of the different fluctuating mechanisms. This is typically accomplished using the triple decomposition (Leschziner, 2016) for every velocity component:

$$u = \underbrace{\underbrace{\bar{u}}_{mean} + \underbrace{u''}_{periodic}}_{phase-averaged,\,\tilde{u}} + \underbrace{u'}_{stochastic} \quad (1)$$

The phase-averaged technique samples, at every point in space, a time series of data obtained for many rotor blade events. Following, the corresponding values for the identical phase (or angular position) of a rotor blade are averaged. The sampling frequency controls the number of phases, or blade positions, (N), being typically in the order of 1 degree per time step. In LES simulations, this selection must be checked with respect to the minimum time step required to capture the turn-out time of the large turbulent eddies (usually limited by the Courant number associated with the grid size). Additionally, the total length of any signal sets the number of blade events stored (M). Note that, in order to obtain a statistically representative averaged signal, the temporal length of the velocity traces has to be extended until the phase-averaged value of the signal is periodic (in other words, M must be sufficiently large).

Figure 3 Schematic for the phase-averaging procedure.

Figure 3 illustrates this methodology to calculate the ensemble-averaged data of the velocity trace (in red), provided in previous figure 2. From the definition of the phase-averaging operator, the phase-averaged value at every angular position (or blade phase in a blade-passing period) is obtained as:

$$\tilde{u}_n^{(M)} = \frac{1}{M}\sum_{m=1}^{M} u_n^{(m)} \quad (2)$$

Where *u* represents the velocity value for every blade event m of the total number (M) of realizations tracked at every point in space. The subindex n indicates every sampled point during the blade passing period. To obtain the turbulence (only the stochastic, random variables), a second-order momentum is thus introduced:

$$\widetilde{u'^2_n}^{(M)} = \frac{1}{M}\sum_{m=1}^{M}\left[u_n^{(m)} - \tilde{u}_n^{(M)}\right]^2 \quad (3)$$

The number of ensemble averages needed to ensure a fully-converged, phase-averaged trace at every point in space is a priori unknown. Consequently, an indicator has to be defined to judge convergence within a predefined confidence level in that unsteady scenario. Inspired by usual CFD practices for stationary turbulent problems, a residual comparing the phase-averaged traces with (M-1) and M ensembles is employed:

$$R^{(M)} = \frac{\sqrt{N\sum_{n=1}^{N}\left[\tilde{u}_n^{(M)} - \tilde{u}_n^{(M-1)}\right]^2}}{\sum_{n=1}^{N}\tilde{u}_n^{(M)}} \quad (4)$$

Note that a summation over all the sampled points is defined in order to obtain a compact value for every angular position. Previous investigations by the authors (Fernández Oro et al., 2015) have shown that there is a correlation between the number of blade events required to ensure a particular convergence criterion and the local, mean-time, turbulence level according to $M \approx \overline{Tu}/R$ where $\overline{Tu} = \frac{\sqrt{N\sum_{n=1}^{N}\widetilde{u'^2_n}^{(M)}}}{\sum_{n=1}^{N}\tilde{u}_n^{(M)}}$

Note that the residual definition requires the computation of the phase-averaged values as defined in eq. (1), which is calculated using all the previous values (i.e., all the instantaneous solutions for every time step had to be stored). In other words, the problem here is the presence of the summation for all the m realizations in the definition of the formulas. Obviously, this is not realizable because of the extremely large amount of data involved, especially for a LES-based simulation with grids up to several million cells and simulation times extended up to several thousand time steps.

Consequently, if the periodic convergence has to be judged on the fly, in the context of practical co-processing, it is necessary to rewrite these expressions to perform just an update on the run. Doing so, the current phase-averaged value has to be recalculated using the present realization (corresponding to the running time step) and the previous ensembled value (which will be replaced with the update). Following, the derivation of these expressions is formally presented.

3.1 Update of the ensemble-averaged value (first moment)

The expansion of eq. (2) for M and (M+1) realizations can be expressed as:

$$\tilde{u}_n^{(M)} = \frac{1}{M}\left(u_n^{(1)} + u_n^{(2)} + \cdots + u_n^{(M)}\right) \quad (5)$$

$$\tilde{u}_n^{(M+1)} = \frac{1}{(M+1)}\left(u_n^{(1)} + u_n^{(2)} + \cdots + u_n^{(M)} + u_n^{(M+1)}\right) \quad (6)$$

Subtracting eq. (5) from eq. (6), the difference of the phase-averaged value calculated with M and (M+1) can be easily obtained after some algebra, yielding:

$$\tilde{u}_n^{(M+1)} - \tilde{u}_n^{(M)} = \frac{1}{M}\left(u_n^{(M+1)} - \tilde{u}_n^{(M+1)}\right) \quad (7)$$

Now, reordering eq. (7), it is possible to update the phase-averaged value for (M+1) realizations using the previous averaged value for M realizations and the new value coming from the current time step:

$$\tilde{u}_n^{(M+1)} = \frac{1}{(M+1)}\left(u_n^{(M+1)} + M\tilde{u}_n^{(M)}\right) \quad (8)$$

As expected, eq. (8) states that the new average is the weighted contribution of the previous averaged value, with a coefficient M/(M+1), and the new value, with a coefficient 1/(M+1). Obviously, as the number of realizations M tends to infinity, the contribution of the new realization becomes irrelevant (i.e., the process has converged).

Additionally, once the phase-averaged value has been updated, it is also interesting to derive the formula for the update of the residual. In this case, due to the RMS value involved in the expression, it is better to reformulate the definition in eq. (4) using eq. (8) to rewrite the quadratic difference, thus resulting:

$$R^{(M+1)} = \frac{\sqrt{N\sum_{n=1}^{N}\left[u_n^{(M+1)} - \tilde{u}_n^{(M+1)}\right]^2}}{M\sum_{n=1}^{N}\tilde{u}_n^{(M+1)}} \quad (9)$$

3.2 Update of the RMS value for turbulence (second moment)

In many situations, not only the convergence of the phase-averaged velocities has to be checked. Turbulent motions can be very intense and significant interaction between the turbulent scales and the periodic unsteadiness can occur. The turbulent scales transported unsteadily by the potential effect of the velocity gradients associated with the blades' displacement, can be reinforced by viscous phenomena, even transferring energy between large scales and turbulent mixing. This is particularly evident at off-design conditions, where turbulent scales exhibit the influence of the blade event after phase-averaging (see the bottom plot in figure 3).

Consequently, it is also necessary to derive a formula for the update of the phase-averaged turbulent kinetic energy given by eq. (3), with its corresponding residual criterion. The convergence of the phase-averaged turbulence (or second-order momentum in the context of the phase-averaging) is thus analyzed in detail. Note that due to the quadratic definition, the mathematical complexity is increased considerably.

Again, the basic idea is to eliminate the summation of all the M realizations in the equations and replace it by the on-going averages modified with the new value. The starting point for the redefinition of eq. (3) is to rewrite the quadratic difference using the relationship shown in eq. (8). It is straightforward to obtain that:

$$\widetilde{u'^2_n}^{(M)} = \frac{1}{M}\sum_{m=1}^{M}\left[\left(u_n^{(m)} - \tilde{u}_n^{(M+1)}\right) + \frac{1}{M}\left(u_n^{(M+1)} - \tilde{u}_n^{(M+1)}\right)\right]^2 \quad (10)$$

The quadratic sum can be expanded to obtain:

$$\widetilde{u'^2_n}^{(M)} = \frac{1}{M}\sum_{m=1}^{M}\left[\left(u_n^{(m)} - \tilde{u}_n^{(M+1)}\right)^2 + \frac{2}{M}\left(u_n^{(M+1)} - \tilde{u}_n^{(M+1)}\right)\left(u_n^{(m)} - \tilde{u}_n^{(M+1)}\right) + \frac{1}{M^2}\left(u_n^{(M+1)} - \tilde{u}_n^{(M+1)}\right)^2\right] \quad (11)$$

Note that the last term in the summation is not depending on the subindex m. The next step is to write the definition in eq. (3) for (M+1) realizations, splitting in two parts:

$$\widetilde{u'^2_n}^{(M+1)} = \frac{1}{(M+1)}\sum_{m=1}^{M+1}\left[u_n^{(m)} - \tilde{u}_n^{(M+1)}\right]^2 = \frac{1}{(M+1)}\left[\sum_{m=1}^{M}\left[u_n^{(m)} - \tilde{u}_n^{(M+1)}\right]^2 + \left(u_n^{(M+1)} - \tilde{u}_n^{(M+1)}\right)^2\right] \quad (12)$$

Following, subtracting eq. (11) from eq. (12), and after some easy algebra, the difference results in:

$$\widetilde{u'^2_n}^{(M+1)} - \widetilde{u'^2_n}^{(M)} = \frac{M^2 - M - 1}{M^2(M+1)}\left(u_n^{(M+1)} - \tilde{u}_n^{(M+1)}\right)^2 - \frac{2}{M^2}\left(u_n^{(M+1)} - \tilde{u}_n^{(M+1)}\right)\underbrace{\sum_{m=1}^{M}\left[u_n^{(m)} - \tilde{u}_n^{(M+1)}\right]}_{(A)} - \frac{1}{M(M+1)}\underbrace{\sum_{m=1}^{M}\left[u_n^{(m)} - \tilde{u}_n^{(M+1)}\right]^2}_{(B)} \quad (13)$$

Some extra work is needed to remove the remaining summations (A) and (B) from eq. (13). Considering that those summations extended to M realizations can be expressed as a function of (M+1) but subtracting the final term, it is quite evident that:

$$\underbrace{\sum_{m=1}^{M}\left[u_n^{(m)} - \tilde{u}_n^{(M+1)}\right]}_{(A)} = \sum_{m=1}^{M+1}\left[u_n^{(m)} - \tilde{u}_n^{(M+1)}\right] - \left(u_n^{(M+1)} - \tilde{u}_n^{(M+1)}\right) \quad (14)$$

And taking advantage one more time of the definition of the phase-averaging operator, the summation for (M+1) can be easily replaced resulting:

$$\underbrace{\sum_{m=1}^{M}\left[u_n^{(m)} - \tilde{u}_n^{(M+1)}\right]}_{(A)} = \sum_{m=1}^{M+1}u_n^{(m)} - (M+1)\tilde{u}_n^{(M+1)} - \left(u_n^{(M+1)} - \tilde{u}_n^{(M+1)}\right) = (M+1)\tilde{u}_n^{(M+1)} - (M+1)\tilde{u}_n^{(M+1)} - \left(u_n^{(M+1)} - \tilde{u}_n^{(M+1)}\right) = \tilde{u}_n^{(M+1)} - u_n^{(M+1)} \quad (15)$$

Similarly, for (B) we use the extension for (M+1) realizations in the case of phase-averaged turbulent kinetic energy, yielding:

$$\underbrace{\sum_{m=1}^{M}\left[u_n^{(m)}-\tilde{u}_n^{(M+1)}\right]^2}_{(B)}=\sum_{m=1}^{M+1}\left[u_n^{(m)}-\tilde{u}_n^{(M+1)}\right]^2 -\left[u_n^{(M+1)}-\tilde{u}_n^{(M+1)}\right]^2= (M+1)\,\widetilde{u'^2_n}^{(M+1)}-\left[u_n^{(M+1)}-\tilde{u}_n^{(M+1)}\right]^2 \tag{16}$$

Finally, introducing eqs. (15) and (16) in eq. (13) and reordering, a definitive expression for the update of the phase-averaged turbulence is finally obtained:

$$\widetilde{u'^2_n}^{(M+1)}=\frac{M}{M+1}\widetilde{u'^2_n}^{(M)}+\frac{M^2+2M-1}{M(M+1)^2}\left(u_n^{(M+1)}-\tilde{u}_n^{(M+1)}\right)^2 \tag{17}$$

In this case, eq. (17) states that the new average is the weighted contribution of the previous averaged value, with a coefficient M/(M+1), and the new value, with a coefficient $(M^2+2M-1)/M(M+1)^2$. Once again, as the number of realizations M tends to infinity, the contribution of the new realization becomes irrelevant.

Finally, once the phase-averaged value has been updated, it is also interesting to derive the formula for the update of the residual. Substituting in the redefinition of eq. (4) for $\widetilde{u'^2_n}$ replacing the M-realization for the new update given by eq. (17), this final expression is obtained:

$$R'^{(M+1)}=\frac{\sqrt{N\sum_{n=1}^{N}\left[\frac{M^2+2M-1}{M(M+1)^2}\left(u_n^{(M+1)}-\tilde{u}_n^{(M+1)}\right)^2-\frac{1}{M}\widetilde{u'^2_n}^{(M+1)}\right]}}{\sum_{n=1}^{N}\widetilde{u'^2_n}^{(M+1)}} \tag{18}$$

4 Numerical database

4.1 Rotor-Stator Model

The mathematical formulation presented here for the analysis of the statistical convergence during co-processing routines in scale-resolving simulations for turbomachinery has been tested using a previous numerical database of the authors.

In particular, a Wall-Modelled LES simulation of the midspan Rotor-Stator (R-S) interaction in a single-stage, low-speed axial fan has been used to check the convergence criterion developed for both phase-averaged velocity and turbulent flow fields.

Results concerning only the midspan section (where both hub and tip end-walls have no significant effect on the bulk flow and the radial velocity is negligible in this free-vortex axial rotor) have been considered in order to exclusively focus on the R-S interaction. With these premises, a 3D extruded linear cascade (with relative motion between rotor blades and stator vanes) was finally modelled with a spanwise extrusion equivalent to one tenth of the blade chord. This allows the preservation of the 3D vortical nature of the vortex shedding throughout the stage.

The airfoil blades are based on the NACA-65-012 class, while the stator vanes are British circular arc profiles C1, with characteristic chord lengths of 150 mm. The axial gap between the rows is 50 mm. The rotating speed of the fan, 2400 rpm, is equivalent to a tangential blade velocity of 75.4 m/s, with a blade passing frequency of 360 Hz. Both nominal (Q_N, corresponding to 43.4 m/s of mean bulk flow velocity) and off-design conditions (70% Q_N, with 30.4 m/s of bulk velocity) were chosen for the analysis. More details can be found in Galdo-Vega et al., 2014.

4.2 Numerical scheme and LES computations

The commercial CFD software FLUENT® was used to solve the full-3D, viscous, filtered Navier-Stokes equations in an unsteady fashion. The basic characteristics of the simulations are summarized in table 3, regarding the geometrical model and boundary conditions, the turbulence closure, the numerical scheme and the computational mesh. Concise details are also given in Fernández-Oro et al., 2019.

Additionally, figure 4 shows a sketch of the modelled 3D cascade (top right), with a general view of the computational mesh. In the bottom part of the figure, several points (P,Q,R,S) and two interrow and outlet rakes (identified as "Upstream" and "Downstream" locations with respect to the stator row) have been selected for the following processing. These lines present a transversal length equal to the vane pitch and are located at one tenth and one fourth of the vane chord from the leading and trailing edges of the vanes respectively.

Table 3 Summary of the CFD simulations.

Numerical model
1. Basic characteristics
• Full-unsteady 3D viscous incompressible flow (sliding mesh technique)
• 3D extruded linear cascade (no hub/shroud endwalls). Up to 3.4 Million cells
• Reduced 3:2 vane-to-blade count ratio (3% pitch modification)
• Time-step: $9.26\cdot10^{-5}$ s, corresponding 30 phases per blade event
• Inlet turbulence: ILS=0.13 m and 1.5% intensity
2. Turbulence closure
• Wall-modelled LES scheme with Smagorinsky Subgrid Scale Modelling
• Mesh requirements in vanes' BLs ($\Delta x^+\sim200$; $\Delta y^+\sim5$; $\Delta x^+\sim150$); i.e. [100x60] O-grid
• Time step for a CFL~2 in the vicinity of vanes; Δx_{cell} ~ 1.5 mm (Re_c = 440,000)
• Roughly 70% of the TKE is resolved in the LES simulation
3. Numerical scheme
• Second-order accurate for the temporal term
• Third-order MUSCL formulation for convection terms
• Second-order accurate, with central difference for diffusive terms
• SIMPLE algorithm for pressure-velocity coupling

Figure 4 Numerical grid and post-processing positions.

To analyze the convergence routines, a total simulation time of 6000 time steps has been considered, thus involving

more than 7.2 Gb of numerical information per working condition. The huge computational requirements needed and the total CPU time required to simulate the unsteady periodic response of the model (up to 450 hours of computation per case) during 200 blade events, illustrates perfectly the need for on-the-run formulations to judge convergence simultaneously and save CPU time and computational resources.

5 Convergence results

5.1 Convergence for first-order moment

Contour maps in figure 5 reveal the phase-averaged temporal evolution (in the x-axis, repeated for convenience) of the velocity distribution (the level contour) at the transversal lines corresponding to the normalized vane pitch (represented between 0 and 1 in the y-axis as *y/w*, being *w* the vane pitch). The velocity maps have been made non-dimensional with respect to the mean bulk velocity of every working condition. In the upstream maps (left side of the figure), for both nominal (top left) and off-design (bottom left) conditions, the periodic arrival of impinging rotor wakes is revealed (marked with black dashed lines). Because of the blade motion, these wakes are oblique as generated by the tangential velocity of the blades in the y-direction.

Figure 5 Phase-averaged velocities upstream and downstream of the vanes. Comparison of nominal and off-design conditions.

Significant intense hot spots are also observed in the upstream maps corresponding to the effect of the stagnation point in the vane leading edge at $y/w \sim 0.4$. It is also interesting to observe the higher disorder in the case of 70% Q_N (the blade wake is more tilted and thicker). Additionally, at downstream locations, the effect of the vane wake is the dominant feature, being clearly evident in the maps. The unmixed rotor wakes, travelling downstream, are still visible but the relevant mechanism is the severe thickening of the vane wake at 70% Q_N as a consequence of the underturned guidance of the flow and the large massive separation on the vane suction side. All these phenomena were already discussed in section 2 to justify the employment of an SRS method.

Figure 6 Convergence histories at different points P,Q,R and S throughout the stage for the velocity field. Comparison of nominal and off-design conditions.

Phase-averaged values shown in figure 5 have been obtained after ensemble-averaging all the available numerical data (200 blade events previously stored) in those lines of interest. To judge the convergence, the histories of the residual at points P, Q, R and S identified in figure 4 are shown in figure 6. As usual, the comparison for both operating conditions is provided. For the analysis, a typical convergence criterion of 10^{-3} has been selected as an accurate threshold that guarantees statistical periodicity (changes below 0.1%). These different points are intentionally placed in those locations where major flow disorder and turbulence generation are expected. Note that at nominal conditions, the convergence criterion is met with a quite reduced number of averages (M<25) for all the points (expect for the point S, within the vane wake). At off-design conditions, the convergence requires a greater number of ensembles due to the higher levels of unsteadiness and turbulent mixing. The typical convergence criterion of 10^{-3} is hardly met for all the points, even using the whole number of blade events recorded. To obtain these figures, eqs. (8) and (9) derived in the mathematical formulation presented in section 3 of the paper have been employed. The evaluation of the residuals has been smoothed using a moving average filter with a span of 10 points to avoid excessive scatter.

In addition, these on-the-run calculations have allowed a significant computational saving of the large amount of data to be post-processed. Precisely, table 4 summarizes the CPU times required to compute the residual histories shown previously (the mean value of the eight traces in figure 6). The evaluation has been calculated in a single PC, intelcore i7-5280K, 3.33GHz with 64 Gb RAM using a postprocessing routine in MATLAB 2019b. The two columns represent the results with the online updating -using eq. (9)-, in comparison to the offline definition -using eq. (4)-, whereas the ratio is shown in the final column. For further insight, the influence of the number of ensembles involved has been also considered, repeating the tests for M=25, 50, 100 and 200 ensembles. In the case of a low number of ensembles (M=25), the post-processing speed is increased by a factor of 4, while for large number of ensembles (M=200), the computational benefit is increased up to 38 times higher. Moreover, it is observed that the computational saving is linearly increased as the required number of ensembles are more demanding.

Table 4 Comparison of CPU times between online updating and offline processing.

Ensembles (M)	Updating CPU time (ms)	Offline CPU time (ms)	Speed ratio
25	0.0111	0.0444	4.0
50	0.0146	0.1242	8.5
100	0.0242	0.4431	18.3
200	0.0431	1.6447	38.2

This CPU times correspond to the convergence history of one single point. The reader can easily understand the importance of this on-the-fly statistics if the region of interest to be ensemble-averaged comprises some million cells. Furthermore, this analysis is not considering the time for I/O read/write operations (or equivalent storing resources in memory) which could dramatically increase the computational cost for offline post-processing.

A complementary representation for the analysis of the convergence is shown in figure 7. In this case, the plots represent, for the whole vane pitch upstream (left) and downstream (right) the number of ensembles required to

attain a particular convergence threshold for the velocity field.

Figure 7 Minimum number of ensemble-averages required to satisfy a given convergence threshold for the velocity field. Comparison of nominal and off-design conditions, upstream (left) and downstream (right) of the vanes.

Upstream, convergence thresholds of $5 \cdot 10^{-4}$ and $2 \cdot 10^{-3}$ are employed to represent the transversal distribution of ensembles required at nominal and off-design conditions. Obviously, off-design results are conditioned by higher levels of unsteadiness. Note that the distributions present a certain degree of blur as a consequence of the inherent instabilities and randomness of the instantaneous velocity values. Whatever the case, coherent structures are predominant, so overall trends are perfectly identified in the distributions. In the right plot, the position of the vane wakes (y/w ~ 0.5-0.6) and their corresponding intensities and widths are clearly evident in the distributions. Central positions of the wakes in the case of partial flow rate (70% Q_N, in red) require an extremely large number of ensembles (>200) to reach the prescribed convergence.

5.2 Convergence for second-order moment

Although convergence for CFD practitioners is generally judged over first-order statistics (i.e., checking that velocity values have reached a sufficiently periodic response), there are situations (especially in case of highly turbulent flows, with massive separations and large-scale fluctuations) in which the convergence of second-order statistics has to be also evaluated.

The flow features for the 70% Q_N of the present numerical database corresponds to one of those situations where overall convergence of the turbulent picture can be compromised using the criterion employed for the velocity fields.

To illustrate the importance of this possibility, the analysis presented in subsection 5.1 is now repeated for the phase-averaged maps of turbulence using previous metrics in a similar way. In figure 8, the phase-averaged values of quadratic velocity fluctuations reveal the incoming wakes upstream and the vane wakes downstream as the main contributors to the turbulent mixing. For the representation, the quadratic periodic fluctuations are expressed in terms of turbulence intensity, according to $\sqrt{\overline{u'^2}}/\bar{\bar{u}}$ where $\bar{\bar{u}}$ stands for the mean bulk flow velocity for every working condition. These metrics illustrate the unsteady (periodic) transport of the coherent turbulent scales of the flow.

Figure 8 Phase-averaged turbulence intensity (%) upstream and downstream of the vanes. Comparison of nominal and off-design conditions.

Concerning the residual histories –computed with eqs. (17) and (18)–, the convergence is significantly retarded due to the inherent instabilities of the coherent turbulent structures. For both nominal and off-design conditions, figure 9 indicates that the typical criterion of 10^{-3} is not reached using the previous value of 200 blade events. An uncertainty of 0.5-1% is characteristic for all the points after using the whole number of realizations available in the database, with minimum residuals in the order of 10^{-2}, especially at off-design conditions.

Figure 9 Convergence histories at different points P,Q,R and S throughout the stage for the turbulence intensity. Comparison of nominal and off-design conditions.

Figure 10 Minimum number of ensemble-averages required to satisfy a given convergence threshold for the turbulence intensity. Comparison of nominal and off-design conditions, upstream (left) and downstream (right) of the vanes.

This section is concluded showing the number of ensemble-averages required for the turbulence to fulfil a convergence threshold of roughly 10^{-2} in all the upstream and downstream locations (figure 10). As expected, the convergence criterion has to be relaxed in order to get a moderate number of blade events, between 100 and 150. Only a significant instability is observed in the distribution at nominal conditions downstream of the vane (black line in the right plot). This effect can be associated with oscillations in the shear layers of the vane wakes. In the other cases, the distributions are quite uniform through the whole vane pitch, thus indicating that phase-averaged large-scale turbulence is not correlated to primary flow variables (wake fluid).

6 Conclusions

Scaled-Resolving Simulations are becoming a feasible option to simulate unsteady flow and turbulence with high accuracy in turbomachinery. Unlike URANS modelling, they do not require a spectral gap between deterministic blade periodicities and large-scale turbulent structures, so they can be applied for all those situations when coupling between both phenomena arise (i.e. multistage environments with R-S interactions). Moreover, these techniques are especially convenient for the analysis of turbomachinery working at off-design conditions, due to their increased ability to describe efficiently the generation of turbulence in case of high swirl motion and massive separation. For LES-based simulations, the most important SRS method so far, requires extremely fine meshes and very reduced time steps, leading to very high computational costs.

In addition, LES resolving provides an inherently unsteady (partly random) solution that must be extended for a wide number of blade events to be statistically representative. Phase-averaging the unsteady turbulent and velocity fields, for at least hundreds of blade passing periods, it is possible to identify the coherent turbulent structures and remove all the randomness embedded in the instantaneous solutions of the flow.

Therefore, a convergence criterion must be defined to satisfy that a certain level of periodic convergence is finally met. When a prescribed threshold is reached, the simulation has been executed for a sufficiently large period of time, so the phase-averaging of all the available data reports an accurate statistical description of the flow fields. However, in most situations, this implies an extremely large amount of data to be stored, which is unrealistic and non-operative in a forward post-processing.

Co-processing has recently emerged as an interesting option for CFD practitioners, where some operations related to the post-processing routines are advanced and introduced during the iterative resolution process of the numerical solver. Deciding in aprioristic basis which is the relevant data for later post-processing, it is more realistic to store only the selected data for a long run until the convergence criterion is fulfilled. Due to the exponential rise of the number of cells in current cutting-edge simulations (up to hundred million cells in most advanced researches), these co-processing techniques are mandatory.

Convergence routines is a basic co-processing technique that allows to stop a long run simulation when the periodic situation has been finally attained. It is necessary to define a number of monitors for convergence to analyze the evolution of the phase-averaging flow as a function of the total number of blade events passed.

In this paper, in order to save computational costs, the mathematical expressions needed to perform the phase-averaging operator on the fly have been formally obtained. The updating of both phase-averaged velocity fields (first momentum) and phase-averaged turbulent intensities (second momentum) have been derived, also defining the expressions for the residual calculation. Moreover, a numerical database of a low-speed, single stage axial fan has been used to apply the mathematical framework presented in the paper. Modelled as a 3D linear cascade (to be focused on the R-S interaction only), the numerical routines for statistical convergence have been presented both downstream and in the inter-row region of the stage.

The need for this co-processing routines and the convenience of using on the fly computations to judge convergence and save computational costs has been demonstrated. The required number of ensembles to ensure convergence was found to be significantly larger at off-design conditions due to the major disorder of the flow patterns. In that situations, the convergence evaluation can be speeded up by a factor of 38 with the updating formulation. In addition, second-order statistics for the turbulent structures have required a larger number of blade events than primary flow variables due to the inherent instabilities of the coherent turbulent structures (hot spots, wake-blade or wake-wake interactions).

References

Adamczyk, J.J. (1999) ‘Aerodynamic analysis of multistage turbomachinery flows in support of aerodynamic design’, *ASME Journal of Turbomachinery*, Vol. 122, No. 2, pp. 189–217.

Benim, A.C., Escudier, M.P., Nahavandi, A., Nickson, A.K., Syed, K.J., Joos, F. (2011) ‘Computational analysis of incompressible turbulent flow in an idealized swirl combustor’. *Progress in Computational Fluid Dynamics*, Vol. 11, No. 1, pp. 42–53.

Chow, Y.-C., Uzol, O. and Katz, J. (2002) ‘Flow nonuniformities and turbulent “hot spots” due to wake-blade and wake-wake interactions in a multi-stage turbomachine’, *ASME Journal of Turbomachinery*, Vol. 124, No.4, pp. 553–563.

Duan, R. et al. (2014) ‘An efficient co-processing framework for large-scale scientific applications’, *Proceedings of the 2014 IEEE 6th International Conference on Cloud Computing Technology and Science*, Singapore, pp. 254–261.

Fernández Oro, J.M., Argüelles Díaz, K.M., Rodríguez Lastra, M., Galdo-Vega, M. and Pereiras García, B. (2014) ‘Converged statistics for time-resolved measurements in low-speed axial fans using high-frequency response probes’, *Experimental Thermal and Fluid Science*, Vol. 54, pp. 71–84.

Fernández Oro, J.M., Meana-Fernández, A., Galdo Vega, M., Pereiras García, B. and González Pérez, J. (2019) ‘LES-based simulation of the time-resolved flow for rotor-stator interactions in axial fan stages’, *International Journal of Numerical Methods for Heat and Fluid Flow*, Vol. 29, No. 2, pp. 657–681.

Galdo-Vega, M., Fernández Oro, J.M., Argüelles Díaz, K.M. and Santolaria Morros, C. (2013) ‘Effect of rotor-stator configuration in the generation of vortical scales and wake mixing in single stage axial fans. Part I: LES modelling and experimental validations’, *Proceedings of the ASME 2013 Fluids Engineering Division Summer Meeting*, Incline Village (Nevada-USA).

Gourdain, N., Sicot, F., Duchaine, F. and Gicquel, L. (2014) ‘Large eddy simulations of flows in industrial compressors: a patch from 2015 to 2035’, *Phil. Trans. R. Soc. A*, Vol. 372: 20130323.

Huang, S., Mohamad, A.A., Nandakumar, K., Ruan, Z.Y., Sang, D.K. (2010) ‘Numerical simulation of unsteady flow in a multistage centrifugal pump using sliding mesh technique’, *Progress in Computational Fluid Dynamics*, Vol. 10, No. 4, pp. 239–245-

Javadi, A. and Nilsson, H. (2015) ‘Time-accurate numerical simulations of swirling flow with rotor-stator interaction’, *Flow Turbulence and Combustion*, Vol. 95, pp. 755–774.

Lehnhauser, T., Ertem-Muller, S., Schafer, M., Janicka, J. (2004) ‘Advances in numerical methods for simulating turbulent flows’, *Progress in Computational Fluid Dynamics*, Vol. 4, No. 3-5, pp. 208–228.

Leschziner, M. (2016) ‘Statistical Turbulence Modelling for Fluid Dynamics – Demystified’, Imperial College Press, London.

Meneveau, C. and Katz, J. (2002) ‘A deterministic stress model for rotor-stator interactions in simulations of average-passage flow’, *ASME Journal of Fluids Engineering*, Vol. 124, pp. 550–554.

Menter, F.R. (2015) ‘Best Practice: Scale-Resolving Simulations in ANSYS-CFD’, ANSYS Inc. Germany GmbH.

Michelassi, V., Wissink, J. and Rodi, W. (2003) ‘Direct numerical simulation, large eddy simulation and unsteady Reynolds-averaged Navier-Stokes simulations of periodic unsteady flow in a low-pressure turbine cascade: a comparison’, *Proceedings of the Imeche – Part A: Journal of Power and Energy*, Vol. 217, No. 4, pp. 403–411.

Tucker, P.G. (2011) ‘Computation of unsteady turbomachinery flows: Part 1 – Progress and challenges”, *Progress in Aerospace Sciences*, Vol. 47, No.7, pp. 522–545.

Tucker, P.G. (2011) ‘Computation of unsteady turbomachinery flows: Part 2 – LES and Hybrids”, *Progress in Aerospace Sciences*, Vol. 47, No.7, pp. 546–559.

Tucker, P.G. (2011) ‘Unsteady Computational Fluid Dynamics in Aeronautics’, Springer, Berlin.

Tucker, P.G. and Tyacke, J.C. (2016) ‘Eddy Resolving Simulation in Aerospace’ – Invited Paper (Numerical Fluid 2014), *Applied Mathematics and Computation*, Vol. 272, pp. 582–592.

Ziegler, B. (2017) ‘Adjoint method-based inverse design of transonic compressor cascade with boundary layer control’, *Progress in Computational Fluid Dynamics*, Vol. 17, No. 6, pp. 335–343.

Figures

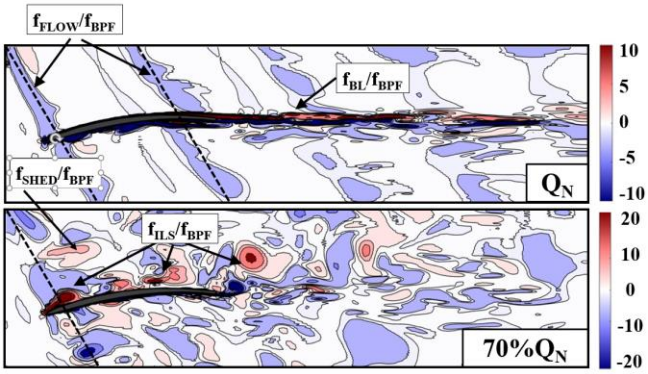

Figure 1 Identification of turbulent structures at nominal (top) and off-design (bottom) conditions.

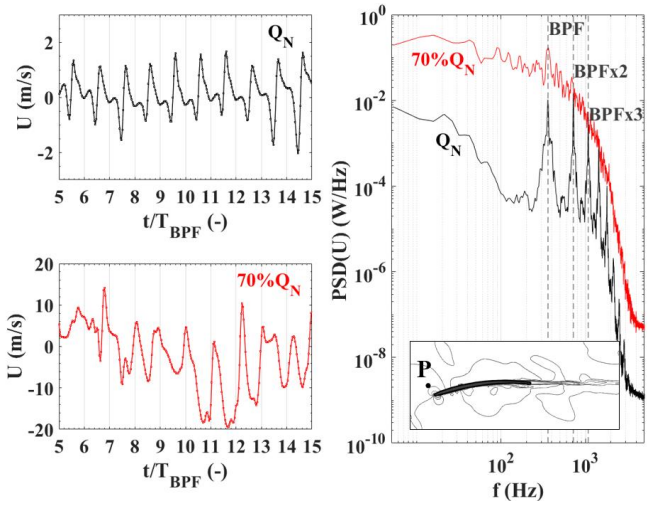

Figure 2 Velocity traces for 10 blade events (left) in a point P close to the vane LE: nominal (top) and off-design (bottom) conditions. Comparison of fluctuating spectra (right). See the point location in the small figure.

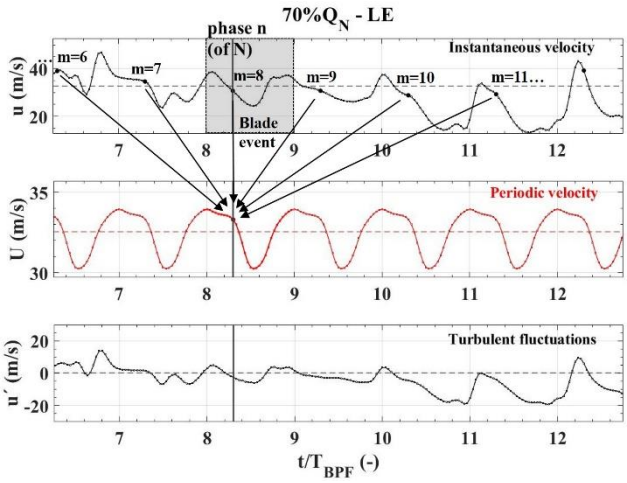

Figure 3 Schematic for the phase-averaging procedure.

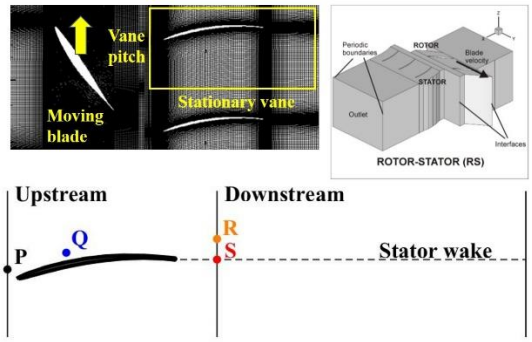

Figure 4 Numerical grid and post-processing positions.

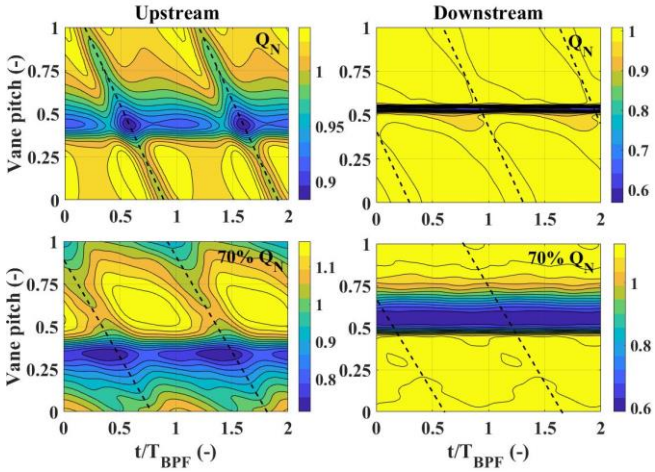

Figure 5 Phase-averaged velocities upstream and downstream of the vanes. Comparison of nominal and off-design conditions.

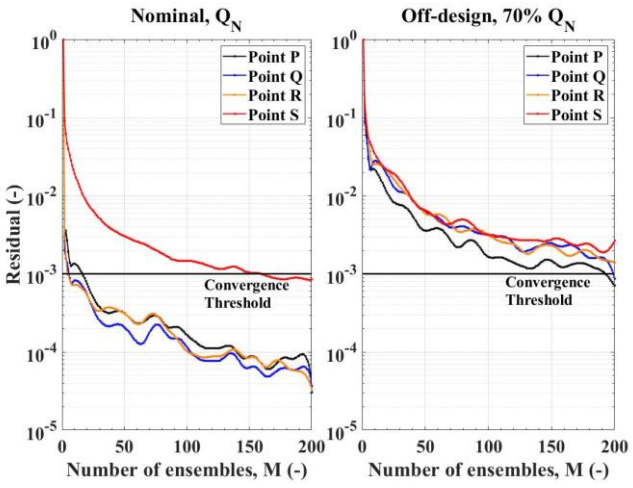

Figure 6 Convergence histories at different points P,Q,R and S throughout the stage for the velocity field. Comparison of nominal and off-design conditions.

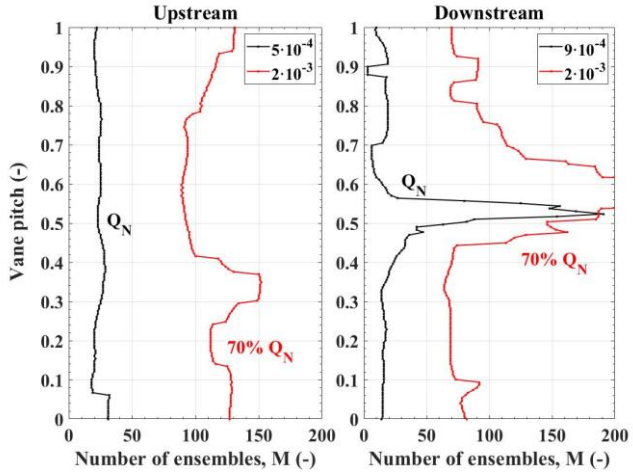

Figure 7 Minimum number of ensemble-averages required to satisfy a given convergence threshold for the velocity field. Comparison of nominal and off-design conditions, upstream (left) and downstream (right) of the vanes.

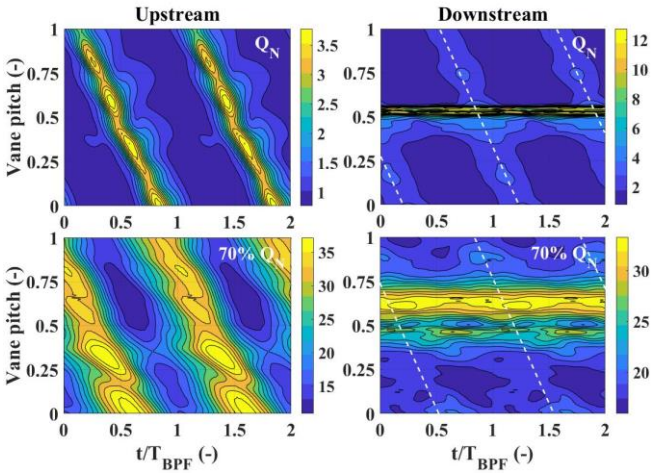

Figure 8 Phase-averaged turbulence intensity (%) upstream and downstream of the vanes. Comparison of nominal and off-design conditions.

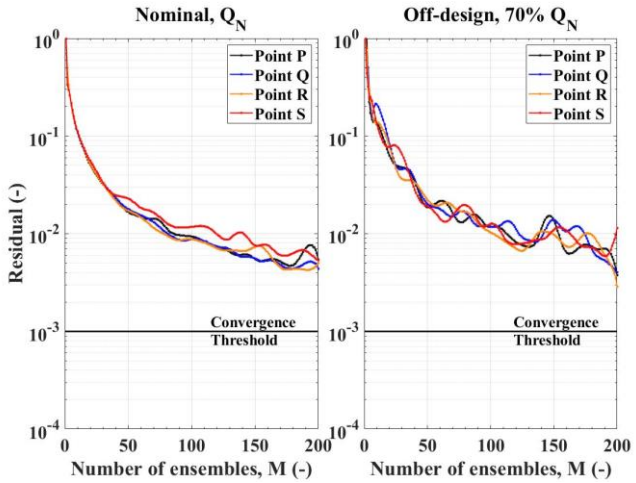

Figure 9 Convergence histories at different points P,Q,R and S throughout the stage for the turbulence intensity. Comparison of nominal and off-design conditions.

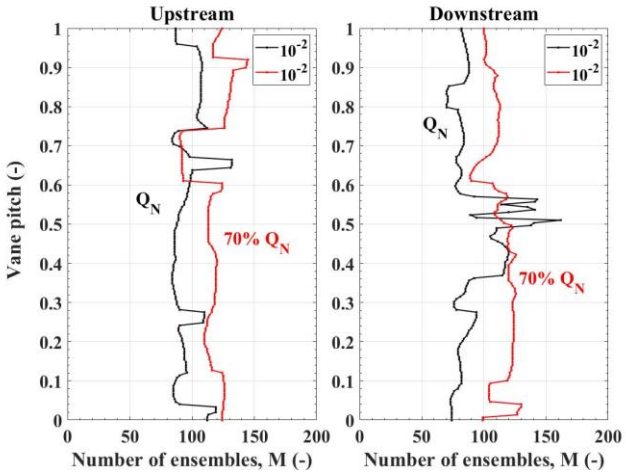

Figure 10 Minimum number of ensemble-averages required to satisfy a given convergence threshold for the turbulence intensity. Comparison of nominal and off-design conditions, upstream (left) and downstream (right) of the vanes.